Chemical Engineering Journal 423 (2021) 129745

Contents lists available at ScienceDirect

Chemical Engineering Journal

journal homepage: www.elsevier.com/locate/cej

Functionalization of biosourced silica and surface reactions with mercury in aqueous solutions

Vassilis J. Inglezakis [a,*], Seitkhan Azat [b,c], Zhandos Tauanov [b,c], Sergey V. Mikhalovsky [d,e]

[a] Department of Chemical & Process Engineering, University of Strathclyde, Glasgow, UK
[b] Faculty of Chemistry and Chemical Technology, Al-Farabi Kazakh National University, Almaty, Kazakhstan
[c] Environmental Science & Technology Group (ESTg), Chemical & Materials Engineering Department, School of Engineering & Digital Sciences, Nur-Sultan, Kazakhstan
[d] ANAMAD Ltd, Sussex Innovation Centre Science Park Square, Falmer, Brighton, UK
[e] Chuiko Institute of Surface Chemistry, National Academy of Sciences of Ukraine, Kyiv, Ukraine

ARTICLE INFO

Keywords:
Biosourced silica
Nanocomposites
Mercury
Calomel
Amalgamation
Hyperstoichiometry

ABSTRACT

This study presents the production of pure silica from rice husk and its stepwise functionalization with triethoxysilane (TES) and silver nanoparticles. The derived TES-SiO_2 (0.97 mmol TES per g of SiO_2) and Ag^0@SiO_2 (3.70–21.60 mg Ag per g of SiO_2) materials were used for the removal of Hg^{2+} from aqueous solutions in the presence of chloride ions. The removal of Hg^{2+} was rapid and the equilibrium solid phase loading was between 21 and 101 mg/g. TES-SiO_2 was more effective than Ag^0@SiO_2 in removing mercury due to the highly reactive hydride groups. In the case of Ag^0@SiO_2 samples the removal of Hg^{2+} is proportional to the amount of Ag^0. The materials were characterized before and after the removal of Hg^{2+} to allow insights into the interaction mechanism. The reaction products for TES-SiO_2 sample were calomel (Hg_2Cl_2) and AgCl. On the surface of Ag^0@SiO_2 samples besides these products the silver amalgams $Ag_{1.1}Hg_{0.9}$ and possibly Ag_2Hg_3 were identified. These results show that redox reactions between silicon-hydride group, Ag^0 and Hg^{2+} take place on the surface of the materials. The coexistence of calomel and silver amalgams on amorphous silica is observed for the first time while the calomel formation in heterogeneous Hg^{2+} redox systems is a rare observation. Also, the samples showed extraordinary efficiency in terms of Hg:Ag molar ratio (2.28–3.02), considerably higher than those reported before. Besides the beneficial effect of the Cl^- presence on the removal of Hg^{2+} from the solution there is evidence of a hyperstoichiometric interaction between Ag^0 and Hg^{2+} at the nanoscale.

1. Introduction

Mercury is a major hazard to atmospheric, soil and water environment and can be found in elemental, inorganic and organic forms. According to UN Environment Programme 2018 assessment on global mercury in total 2,223 tons were discharged from anthropogenic activities [1]. The stationary combustion of fossil fuels and biomass is responsible for approximately 24% of mercury emissions to the atmosphere, primarily from coal burning (21%), with other major mercury emissions originating from non-ferrous metal (15%) and cement (11%) production [1,2]. Mercury may cause serious health issues even at relatively low concentrations and diseases may include damage of brain and kidneys, nervous and endocrine systems [3,4]. The famous "Minamata disease" caused by mercury release into the water was widely spread in Japan in 1950s [5]. This alarming disaster triggered an urgent need for regulation and management of anthropogenic waste mercury. As a result, the Minamata Convention on Mercury in 2013 was signed and became effective in 2017 and to date 127 countries have entered the agreement [2,5].

The hazardous and acute toxic mercury species (both organic and inorganic) require cost-effective and efficient technologies that can be easily scaled-up. To reach this goal, a number of mercury removal methods from flue gases and wastewater have been investigated. The most common methods are adsorption [6-8], ion exchange [9,10] and membrane separation [11,12] with electrochemical methods recently attracting more attention [13]. Several adsorbents such as synthetic and natural zeolites [14-16], graphene and activated carbons [17,18], metal and covalent organic frameworks [19-21] and other functionalized polymers [22] have been extensively studied. An alternative option is silica, a robust material with high surface area, easily synthesized or

* Corresponding author.
E-mail address: vasileios.inglezakis@strath.ac.uk (V.J. Inglezakis).

https://doi.org/10.1016/j.cej.2021.129745
Received 12 February 2021; Received in revised form 2 April 2021; Accepted 6 April 2021
Available online 5 May 2021

produced from natural sources such as rice husk. Rice husk (RH) is an agricultural by-product and an abundant source of both silica and activated carbon depending on processing conditions [23,24]. For example, silica derived from RH has been utilized in the catalytic degradation of dyes [25] and removal of Pb^{2+} [26] and drugs [27] from water, while RH-derived activated carbon has been employed for the removal of Cu^{2+}, NO_3^- [28,29] and of volatile organic compounds from water [30]. Surface functionalization of an adsorbent is often a necessary step for many applications[31]. In general, functionalization leads to incorporation of active groups on the surface of the adsorbent for enhancing its affinity toward certain molecules or ions. For the removal of metals from aqueous solutions, SiO_2 can be functionalized with amine, thiol [32] and silicon-hydride groups [33]. Concerning the later, the chemicals most commonly used are (3-aminopropyl) triethoxysilane (APTES), (3-mercaptopropyl) trimethoxysilane (MPTMS) and triethoxysilane (TES). An advantage of TES is that its redox active fragment offers a simpler chemistry without bridging $–CH_2–$ groups to the silicon atom.

Mercury exhibits the unique ability of forming alloys called amalgams at ambient temperature with most metals, the most common being the Hg-Ag amalgams. Amalgams have several applications due to their chemical, electronic and optical properties [4]. Taking advantage of the amalgamation reaction, adsorbents can are impregnated with metallic silver for the selective removal of mercury from aqueous solutions [14,20]. Besides the synthesis of such smart mercury scavengers other applications include the development of optical probes for ultrasensitive Hg^{2+} detection [4]. Despite the strong interest in mercury removal from water, few studies have been published on the interaction of Hg^{2+} with TES- or Ag^0-functionalized SiO_2 and none on their comparison (Table 1). The removal of mercury from $HgCl_2$ solutions by silica-based materials has not been studied in depth either. Katok *et al.* [34] used $Hg(NO_3)_2$ and $Hg(OAc)_2$ solutions while Yordanova *et al.* [35] studied the influence of NO_3^- and Cl^- but the nanocomposite used besides Ag^0 nanoparticles (NPs) was decorated with NH_2 groups which contributed to the removal of Hg^{2+}. Ganzagh *et al.* [36] used $HgCl_2$ but did not provide any insights on the nature and composition of the compounds or the surface complexes formed. Azat *et al.* [37] used a very similar SiO_2 sample and $HgCl_2$ solutions but the limited removal experiments and inconclusive XRD data did not allow in-depth analysis of the surface reactions. The interest in $HgCl_2$ solutions is related to the existence of different aqueous Hg^{2+}-Cl^- species and the potential formation of calomel (Hg_2Cl_2) which has both environmental and industrial significance [38].

Herein, we report the continuation of our previous work on RH-derived silica [37,39]. In this work, biosourced silica is produced from RH, functionalized with TES and Ag^0 NPs and then used for the removal of Hg^{2+} from water. The removal of mercury from aqueous solutions containing Cl^- ions by use of the RH-derived silica, TES-functionalized and Ag^0-modified silica is presented and discussed. Advanced characterization methods were used for the characterization of on the pre- and post-adsorption materials complemented with speciation studies of mercury species in water and a detailed plausible removal mechanism is presented.

Table 1
Literature review on aqueous phase Hg-Ag interaction on the surface of SiO_2 functionalized with TES and Ag^0 NPs.

Solid phase and SiO_2 type	Liquid phase[1]	Formed compounds/ substances	Reference
TES-SiO_2	$Hg(NO_3)_2$	Hg_2^{2+}/Hg^{2+} surface complexes	[33]
Fumed silica (Cab-o-sil)	C_o = 1.4–8 ppm pH_o = 2–11		
Ag^0@SiO_2 Amorphous (synthesized from rice husk)	$HgCl_2$ C_o = 100 ppm pH_o = 4–5	Ag_2Hg_3 Ag_3Hg Hg_2Cl_2 HgO AgCl AgO	[37]
Ag^0 NPs@SiO_2 Fumed silica (C-120)	$Hg(NO_3)_2$ $Hg(OAc)_2$ C_o = 0.15–312 ppm pH_o = 4–7	$Ag_{1.1}Hg_{0.9}$	[34]
Ag^0@ SiO_2 Amorphous	Hg^{2+} with HNO_3/HCl C_o < 10 ppb pH_o = 2–7	Ag_2Hg_3 Hg^0	[35]
Ag^0@SiO_2 Amorphous (synthesized SBA-15)	$HgCl_2$ C_o = 50–200 ppm pH_o = 3.5–7	Not specified	[36]
TES-SiO_2 Ag^0@SiO_2 Amorphous (synthesized from rice husk)	$HgCl_2$ C_o = 300 ppm pH_o = 5.5	Ag_2Hg_3 $Ag_{1.1}Hg_{0.9}$ Hg_2Cl_2 AgCl	This work

[1] C_0 – initial mercury concentration, pH_o – initial pH

2. Materials and methods

2.1. Materials and chemicals

Triethoxysilane (TES, Sigma Aldrich, 390143, 95%), acetic acid (glacial), concentrated hydrochloric acid, silver nitrate and mercury (II) chloride were purchased from Sigma Aldrich and used without further purification. RH sourced from South Kazakhstan was used as the precursor material for the silica synthesis. Ultrapure water (UP) of 18.3 MΩ·cm resistivity was used for preparing all solutions.

2.2. Synthesis of nanocomposites

2.2.1. Synthesis of silica

Pure silica was produced following the method presented elsewhere [39]. In brief, following washing with water and drying of the raw material the samples were calcined and the resulting solids were treated with NaOH under stirring to extract the solid silica into water-soluble sodium silicate. After filtration, the sodium silicate solution was converted into insoluble silicic acid via reaction with concentrated HCl under continuous stirring. Finally, the precipitated silica was washed and dried. The resulting material was named RH-SiO_2.

2.2.2. Silica modification by TES

3 g of the RH-SiO_2 sample was added into a round bottom flask equipped with a reflux condenser. The flask was placed in a water bath with constant temperature (90 °C) and a solution of 0.46 mL of triethoxysilane (TES) in 60 mL of the glacial acetic acid was added under continuous stirring. After 2 h of reaction, the mixture was cooled to room temperature and filtered. The obtained material was dried at 90 °C. The resulting modified silica samples were used for immobilization of Ag^0 NPs. The modified silica material was named TES-SiO_2. The concentration of silicon-hydride (≡Si-H) groups was measured by iodometric titration [40]. The method is based on the redox reaction between I_2 and ≡Si-H and subsequent titration of the non-reacted I_2 with $Na_2S_2O_3$. All measurements were done in triplicate and the average values are reported.

2.2.3. Immobilization of silver nanoparticles

1.1 g of TES-SiO_2 sample was immersed in different volumes of 15.46 mM aqueous silver nitrate solution at ambient temperature to synthesize three different SiO_2 samples with immobilized silver NPs; sample A (66 mL), sample B (22 mL) and sample C (11 mL). The modification was carried out in dark to prevent oxidation of silver. Ag^0 NPs are formed on the surface of silica through chemical reduction of

silver ions into zero-valence state as result of the reaction with silicon-hydride groups. The obtained samples were thoroughly washed, filtered and dried for 12 h at 105 °C in a bench oven. The resulting nanocomposites were named $Ag^0@SiO_2$.

2.3. Mercury removal experiments

The $Ag^0@SiO_2$ nanocomposites and the TES-SiO_2 samples were tested for the removal of mercury from $HgCl_2$ solution of 300 mg/L concentration without pH adjustment at ambient temperature. In all experiments 0.1 g of the adsorbent was added in a conical flask containing 40 mL of $HgCl_2$ solution. The mixture was left to react until equilibrium was reached (96 h). The samples were centrifuged and the solutions were analyzed for mercury. The kinetic experiments were repeated two to four times and the average standard deviation was 5.9%.

The amount of mercury adsorbed was calculated from the difference between its initial and final concentrations in the solution according to the equation (1):

$$q_{eq} = \frac{c_o - c_f}{m} \times V \quad (1)$$

where q_{eq} is the mercury loading on the material (mg/g), C_o and C_f are the initial and final mercury concentrations (mg/L) respectively, V the volume of the solution (L) and m is the initial weight of the solids (g). To avoid confusion, throughout the paper the term "loading" and symbol q (mg/g) are used to describe the amount of species adsorbed per initial weight of the solid phase (before adsorption) and the term "content" and symbol ct (mg/g) to describe the amount of species adsorbed per total weight of the solid phase (initial weight plus the weight of the adsorbed species). The former is typically used for kinetic and equilibrium studies while the latter for XRF, EDX and other compositional analyses. Loading and content are related as follows:

$$ct = \frac{q}{1 + \left(\frac{q}{1000}\right)} \quad (2)$$

2.4. Materials characterization and analytical methods

The characterization of SiO_2 and TES-SiO_2 was reported elsewhere and only characterizations essential to this study are presented here [37]. Fourier Transform Infrared Spectra (FTIR) were recorded on Cary 600 series FTIR spectrometer (Agilent Technologies), in transmission (T) mode at wavenumbers range 500–4000 cm^{-1} with a resolution of 2 cm^{-1}. The chemical composition of the samples was determined by X–ray fluorescence (XRF) on an Axios Max (XRF, PANalytical) operating with Rh X-ray tube and four analyzing crystals, namely LiF200, PE002, PX1 and LiF220. XRF characterization was done twice for each sample and the averages are reported. X-ray diffraction (XRD) patterns were recorded using a SmartLab® X-ray diffraction system (Rigaku) with Cu Kα radiation source (λ = 1.54 Å) at a scan rate of 0.02° $\theta \cdot s^{-1}$. The morphological characteristics of samples were studied by scanning electron microscopy (SEM) using a JEOL 6380LV Scanning Electron Microscope, operating in LV mode, at 20 kV, equipped with a back-scattered electron detector. Mapping analyses were carried out using a Si (Li) Energy-Dispersive X-ray spectrometer INCA X-sight (Oxford Instruments) connected to SEM. Transmission Electron Microscope (JEOL JEM-2100 LaB6) was employed to investigate the morphology and size of the synthesized silver NPs. The mercury concentration in aqueous samples was analyzed by a RA-915 M Mercury Analyzer (Lumex-Ohio) with a pyrolysis attachment (PYRO-915^+). After silica modification with silver the supernatant solutions were analyzed for silver by Atomic Absorption Spectrometer (AAnalyst 400, Perkin Elmer).

3. Results and discussion

3.1. Characterization of materials

The hydride content measured by iodometric titration was 0.05 ± 0.02 mmol/g for SiO_2 and 0.97 ± 0.19 mmol/g for TES-SiO_2, which confirms successful modification of TES-SiO_2 with ≡Si-H groups. The ≡Si-H groups were detected in FTIR spectra at 2271 cm^{-1} (Fig. 1). The number of silanol groups per unit of surface, when the surface is fully hydroxylated is considered to be a physicochemical constant. This constant, on average, has a numerical value of 4.6 OH-groups per nm^2 and is known in the literature as Kiselev–Zhuravlev constant [41]. The BET surface area of the SiO_2 sample used is 980 m^2/g [39] and thus the concentration of silanol groups is 7.03 mmol OH/g silica. Assuming that one TES molecule binds to the silica surface via three OH– groups, ca. 41.40% conversion of OH– into ≡Si-H was achieved assuming that the silica used was fully hydroxylated. FTIR shows a reduction of the intensity of the broad silanol OH band with the peak at around 3500 cm^{-1} but this method is only offers a semi-quantitative indication.

The silver content measured by XRF was 2.16 ± 0.19% w/w in sample A, 0.98 ± 0.08% w/w in sample B and 0.37 ± 0.04% w/w in sample C. These values are considerably lower than those calculated by analyzing the solutions for silver after the modification of silica, namely 7.97% w/w, 3.20% w/w and 1.64% w/w, respectively. This shows that a significant amount of Ag^0 was not strongly attached to silica surface and was removed after washing the materials. Visual observation of samples showed that SiO_2 and TES-SiO_2 samples have white color while $Ag^0@SiO_2$ samples are dark brown and become lighter in color as the silver content is decreasing (Fig. 2).

The XRD spectra are shown in Fig. 3. The peaks at 38.1°, 44.3°, and 64.5° are characteristic of metallic Ag^0 (PDF card 0–001-1164). Using the Scherrer equation and the peak at 38.1° the size of Ag^0 NPs was estimated at 22–25 nm for all samples.

The TEM images of $Ag^0@SiO_2$ samples clearly show spherical nanoparticles of variable sizes (Fig. 4), which is in a reasonable agreement with XRD results.

3.2. Adsorption kinetics and mechanism

The removal kinetics are presented in Fig. 5. The major part of Hg^{2+} is removed after 8 h for all samples. The removal efficiency is decreasing in the following order (in parenthesis the equilibrium solid phase loading): TES-SiO_2 (101 mg/g) > sample A (91 mg/g) > sample B (48 mg/g) > sample C (21 mg/g) > SiO_2 (6.9 mg/g).

The results show that TES-SiO_2 is an effective adsorbent owing to the ≡Si-H groups. However, the ≡Si-H groups are not stable in alkaline and slightly acidic solutions and react with water [33,42]:

$$\equiv SiH + H_2O \rightarrow \equiv SiOH + H_2 \quad (1)$$

If some of ≡Si-H groups remain on the materials after the silver modification then they should be in higher concentrations in sample C, followed by sample B and sample A, contributing to the removal of mercury. Without excluding this possibility, the results show that the removal effectiveness of $Ag^0@SiO_2$ samples is proportional to Ag^0 content and thus it is silver content that determines the removal of mercury.

The XRD results are presented in Figs. 6 and 7. The SiO_2 sample showed only the characteristic broad peak of amorphous silica at 22°. The rest of samples showed peaks at 21.4°, 28.2°, 31.8°, 32.9°, 40.2°, 43.9°, 46°, 53° and 58.2°, which are characteristic of Hg_2Cl_2 (PDF card 00-001-0768). The $Ag^0@SiO_2$ samples showed additional peaks at 32.3°, 54.9° and 57.5° characteristic of AgCl (PDF card 00–001-1013). After mercury adsorption all samples were white except sample A, which showed two distinct phases, a white (sample A(W)) and a denser black

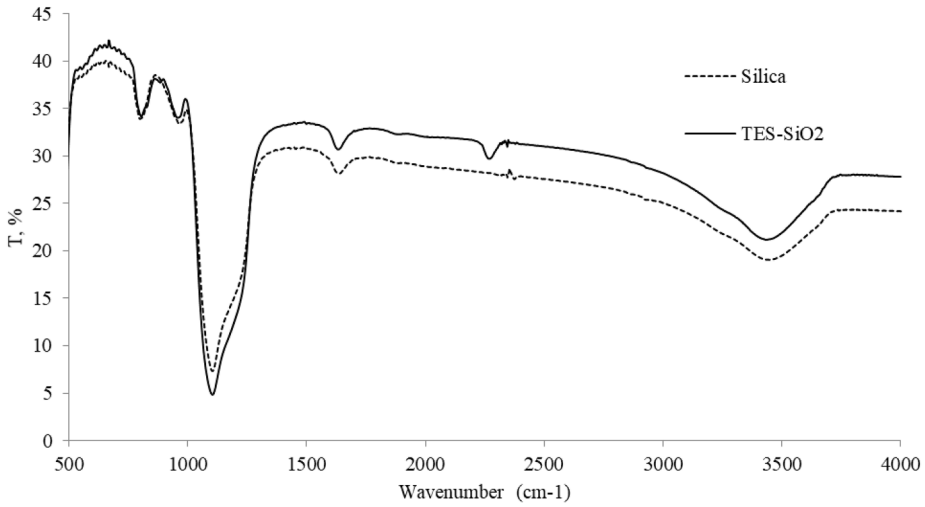

Fig. 1. FTIR spectra of silica and TEOS-modified silica.

Fig. 2. Appearance of the materials, from left to right: SiO_2, TES-SiO_2, sample A, sample B and sample C.

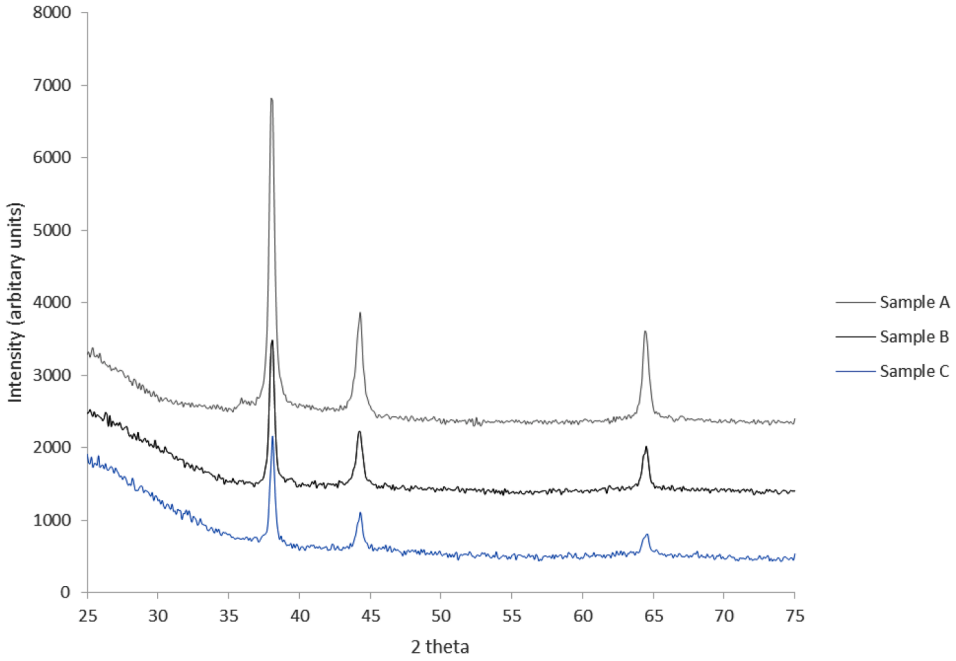

Fig. 3. XRD patterns of the Ag^0@SiO_2 samples.

phase (sample A(B)) (Fig. 8). Calomel is white to grey while amalgams are dark grey to black. Sample A(B) shows additional peaks at 34.6°, 37.2° and 39.6°, characteristic of schachnerite $Ag_{1.1}Hg_{0.9}$ (PDF card 00-027-0618), which has silver-grey color, and at 38.1°, characteristic of metallic silver Ag^0 and silver-white moschellandsbergite Ag_2Hg_3 (PDF card 00-011-0067). Thus, the color of the samples qualitatively corroborates the XRD results.

To the best of own knowledge, with the exception of the paper by Azat *et al.* [37], in which XRD results were inconclusive, this is the first time when coexistence of Hg_2Cl_2 and Hg-Ag amalgams is observed on silica materials and a proof of a simultaneous reduction of Hg^{2+} to Hg_2^{2+} and Hg^0 in heterogeneous Hg^{2+} redox systems. Also, the formation of calomel is rarely reported in such systems, for instance see the work of Pasakarnis *et al.* on magnetite [43] and more recently of Tauanov *et al.* on synthetic zeolite Ag-nanocomposites [44].

The silver and mercury content of the samples before and after

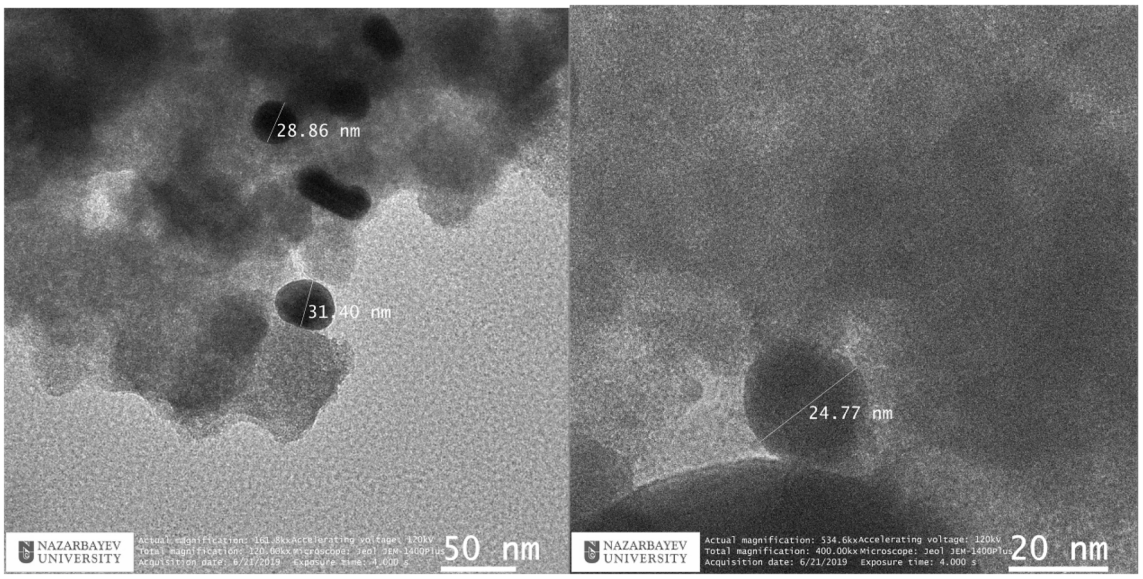

Fig. 4. Representative TEM images of sample A (left) and sample B (right).

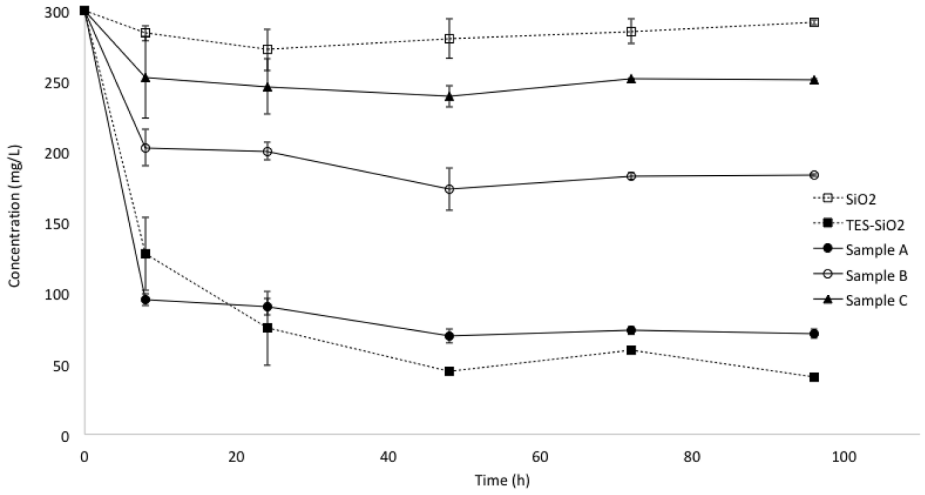

Fig. 5. Kinetics of Hg^{2+} removal by silica-based materials (error bars represent standard deviation).

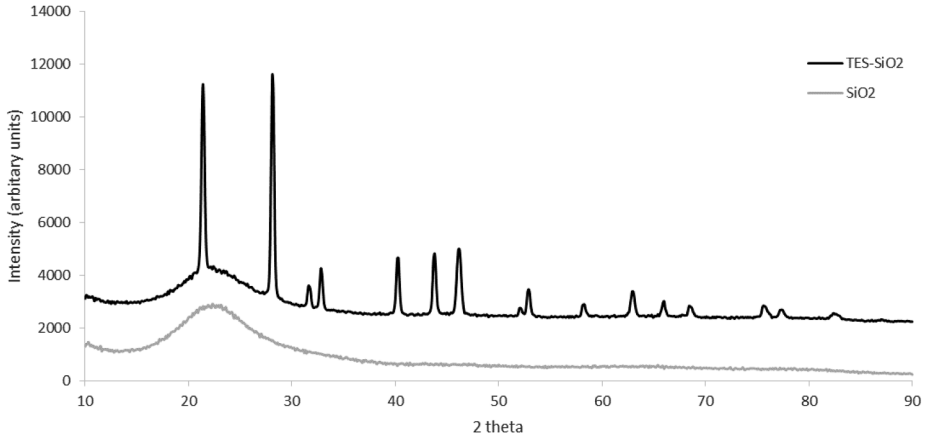

Fig. 6. XRD analysis of SiO_2 and TES-SiO_2 samples after mercury adsorption.

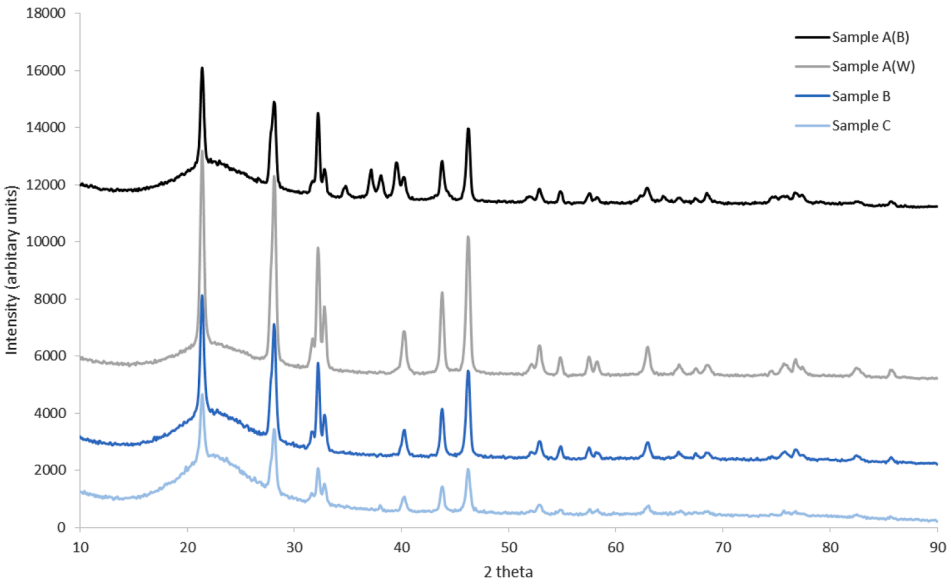

Fig. 7. XRD analysis of $Ag^0@SiO_2$ samples after mercury adsorption.

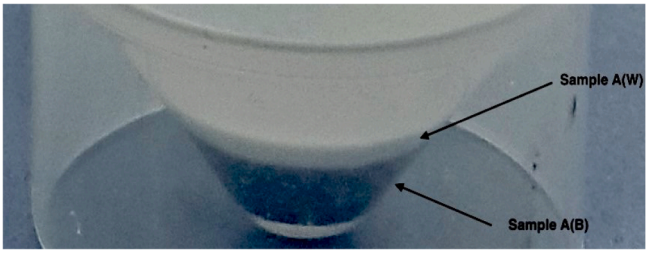

Fig. 8. Photo of sample A after mercury adsorption showing the two separate layers of solid at the bottom of the tube.

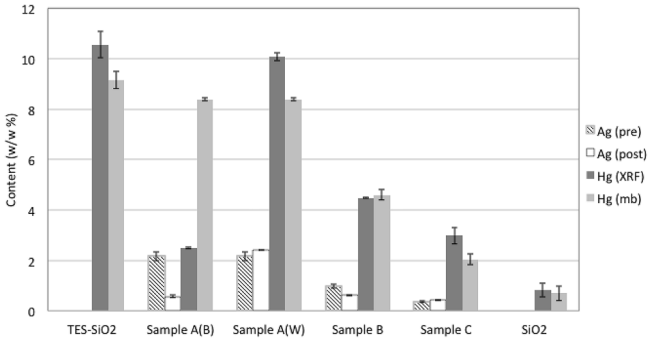

Fig. 9. Silver and mercury content before and after adsorption (error bars represent standard deviation).

adsorption measured by XRF are presented in Fig. 9. The Hg(mb) is the mercury content calculated by material balance as a difference in its concentration in solution before and after adsorption. The Hg(mb) in sample A refers to the mixed material (B and W) and thus represents an average value. It is evident that XRF analysis confirms the existence of mercury on all samples and provides the expected trend and content values close to those calculated by material balance. Also, taking into account the semi-quantitative nature of XRF measurements, the silver content before and after adsorption remains practically unchanged. The exception is the XRF analysis of sample A(B) after adsorption, which showed much less silver and mercury, which is an indication of amalgam formation. Amalgamation is expected to be slower process than precipitation of calomel leading to lower Hg content. Also, probably Hg and Ag are partially lost during XRF characterization. Calomel has a melting point of 525 °C while, based on Hg-Ag phase diagrams, liquid schachnerite and moschellandsbergite with mercury content of approximately 60% w/w and 73% w/w appears in considerably lower temperature at 276 °C [45].

The results of SEM/EDX analyses are shown in Fig. 10. On TES-SiO_2 sample Hg coexists with Cl as expected due to the formation of Hg_2Cl_2. On silver samples, Ag, Hg and Cl are observed on the surface of the solids and Ag and Cl, and Hg and Cl coexist supporting the XRD observations on the formation of AgCl and Hg_2Cl_2.

TEM images of $Ag^0@SiO_2$ samples after mercury adsorption showed spherical nanoparticles, most probably Ag^0 and dark spots attributed to Hg_2Cl_2 and AgCl formation (Fig. 11). The size of Ag^0 NPs is smaller than in the initial $Ag^0@SiO_2$ samples before mercury adsorption and can be a result of partial oxidation and dissolution of silver during mercury adsorption. Liu *et al.* studied the formation of Hg-Ag nanoalloys starting from Ag^0 NPs of different shapes and liquid Hg^0. Their data showed that the resulting spherical schachnerite nanoparticles were larger than the initial Ag^0 NPs [46]. Katok *et al.* also found that schachnerite NPs formed on $Ag^0@SiO_2$ had larger size than initial Ag^0 NPs however their shape was irregular. In the present work the hexagonal nanoparticles observed on sample A(B) (Fig. 12) can be attributed to the formation of schachnerite, zeta (ζ) phase [47]. This is a rare finding and in agreement with the XRD results, however in the absence of TEM/EDX analysis it is not conclusive. Finally, no Hg_2Cl_2 nanoparticles were observed on the surface of TES-SiO_2. The synthesis of free Hg_2Cl_2 nanoparticles was for the first time reported by Bartlett *et al.* [38].

The electrochemistry and chemical speciation of mercury in aqueous solutions are complex and although the reduction of Hg^{2+} has been the subject of a number of studies there is no general agreement as to whether the reduction occurs in one or two stages through the production of Hg_2^{2+}. Obviously, the reduction to Hg_2^{2+} is particularly important, especially in the presence of Cl^- as it can result in the formation of calomel (Hg_2Cl_2) inhibiting further reduction to Hg^0 and the formation of amalgams in the presence of Ag^0. Katok *et al.* [33] used $Hg(NO_3)_2$ and TES-SiO_2 and found that Hg^{2+} is reduced to Hg_2^{2+} and excluded the formation of Hg^0. In another study Katok *et al.* [34] used $Hg(NO_3)_2$, Hg $(OAc)_2$ and $Ag^0@SiO_2$ and no Hg_2^{2+} was detected. However, there is no fundamental reason for Ag^0 to not reduce Hg^{2+} to Hg_2^{2+} as in the case of H^- as this is possible according to the redox potentials shown below:

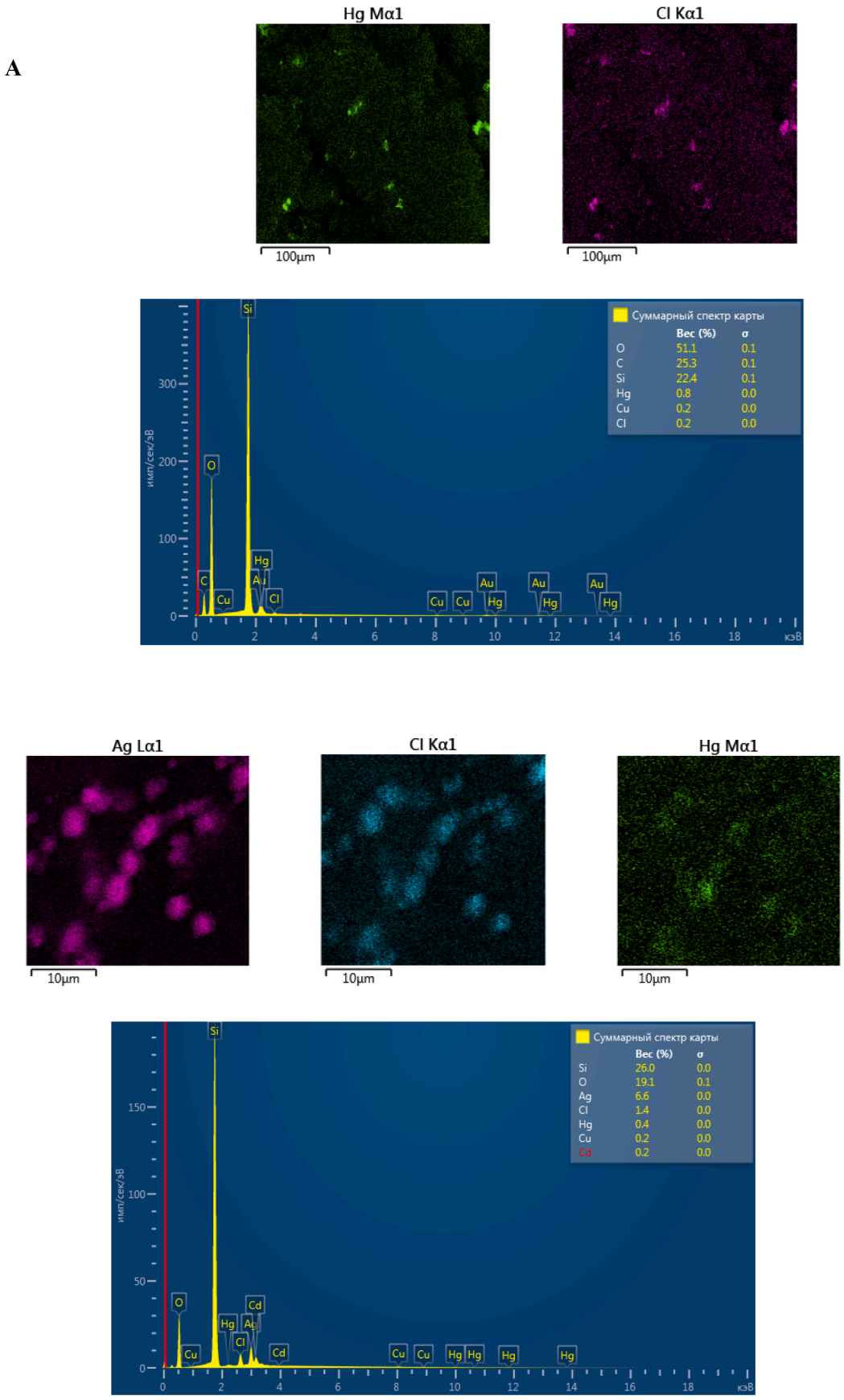

Fig. 10. SEM/EDX analysis of adsorbents after mercury adsorption: (A) - TES-SiO_2, (B) - Sample A(B), (C) - Sample A(W) and (D) - Sample B (elemental analysis results are not normalized). For each sample SEM micrographs are followed by EDX spectra.

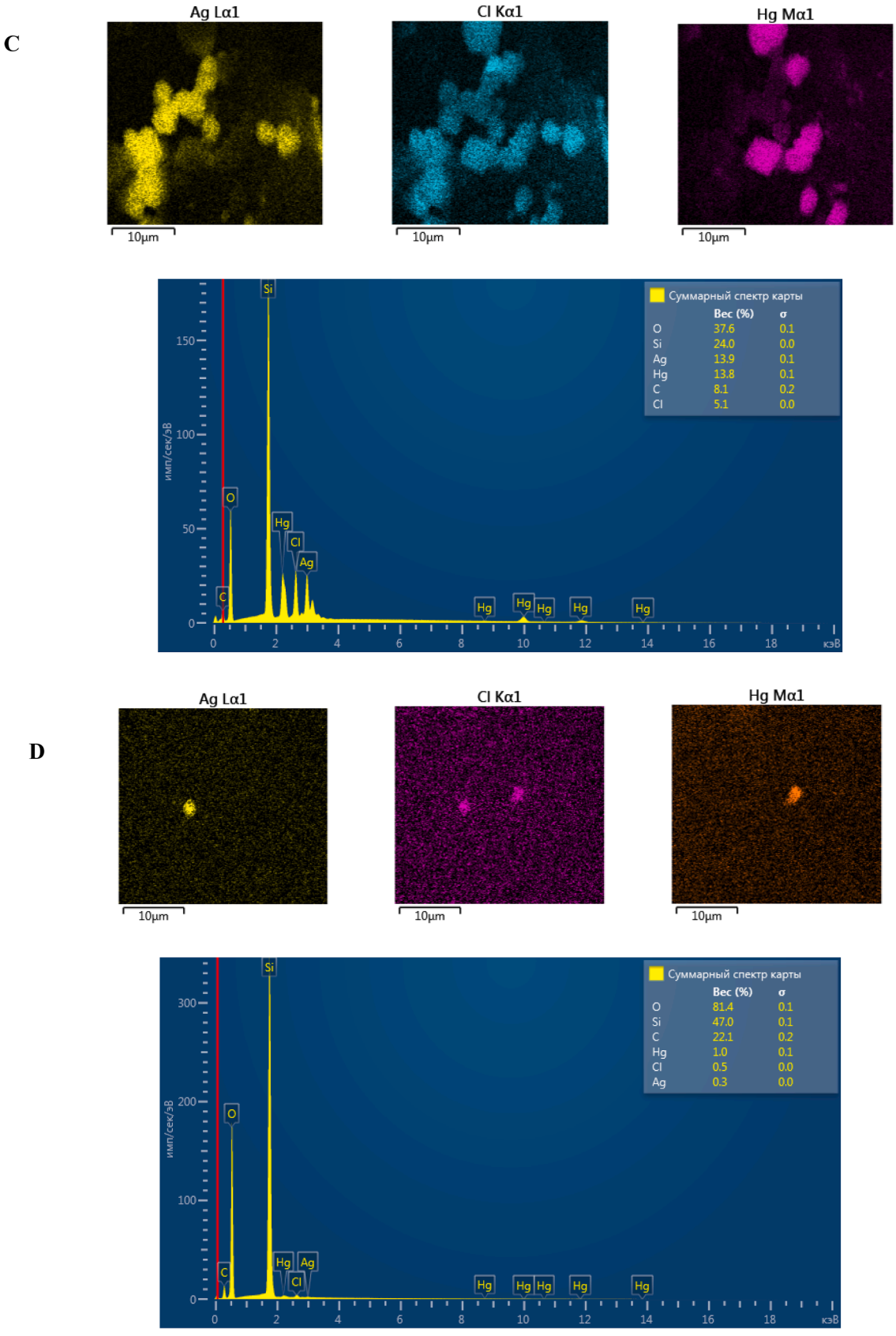

Fig. 10. (*continued*).

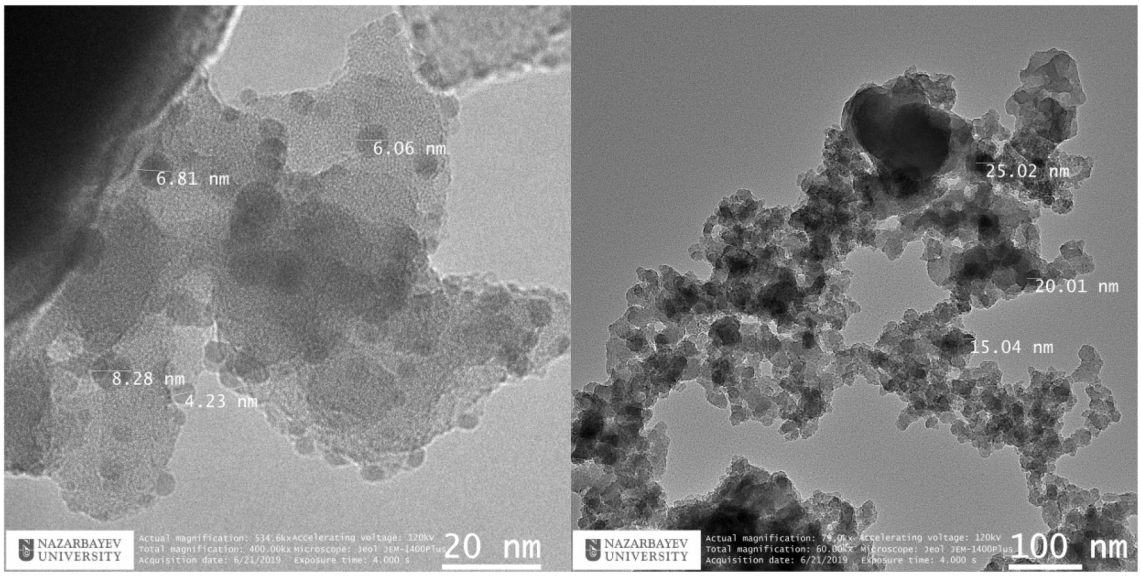

Fig. 11. TEM images of sample A(W) (left) and sample B after mercury adsorption.

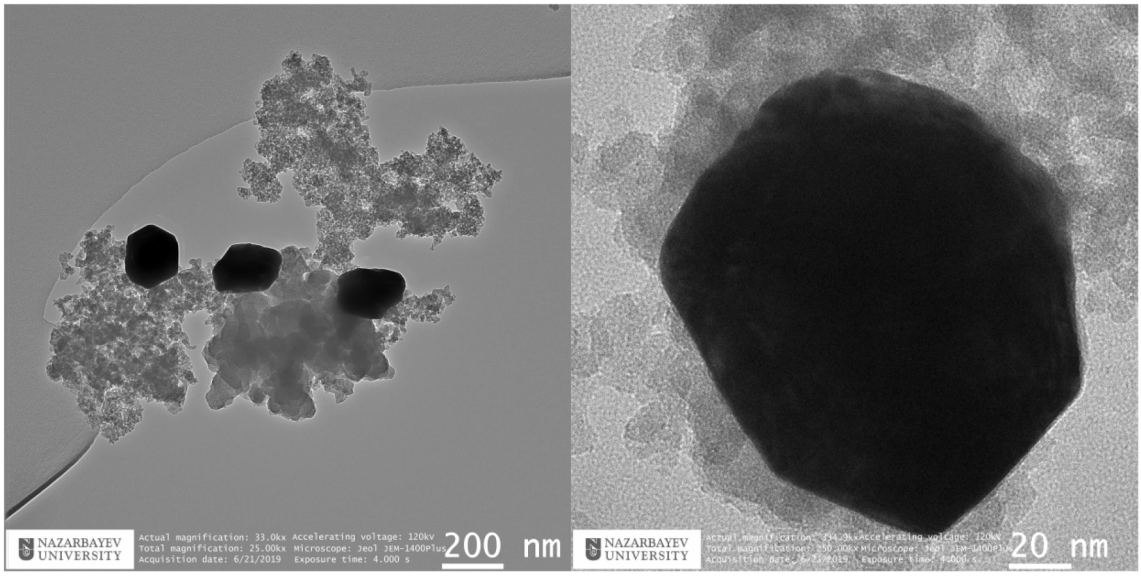

Fig. 12. TEM images of sample A(B) after mercury adsorption.

$H_2 + 2e^- \rightleftharpoons 2H^-$ −2.25 V

$Hg_2Cl_2 + 2e^- \rightleftharpoons 2Hg^0 + 2Cl^-$ +0.27 V

$Hg_2^{2+} + 2e^- \rightleftharpoons 2Hg^0 + 0.80$ V

$Ag^+ + e^- \rightleftharpoons Ag^0 + 0.80$ V

$Hg^{2+} + 2e^- \rightleftharpoons Hg^0 + 0.85$ V

$2Hg^{2+} + 2e^- \rightleftharpoons Hg_2^{2+}$ +0.92 V

Although it is rarely discussed in the literature, Hg^{2+} in $Hg(NO_3)_2$ and especially $HgCl_2$ solutions is mainly found in the form of Cl^- and OH^- complexes (Fig. 13). Thus, it is assumed that either these complexes allow redox reactions to happen or are weak enough for free Hg^{2+} to be available [44].

The silicon-hydride group in TES-SiO_2 sample is not as strong a reductant as in boron-hydride groups or metal hydrides for which the redox potential of −2.25 V has been estimated [48], but it can reduce both Ag^+ and Hg^{2+} to form Ag^0@SiO_2 and Hg_2^{2+} [33,34]. Previous studies have shown that the reduction of Hg^{2+} on the surface of TES-SiO_2 does not proceed to Hg^0 [33]. Thus the proposed reactions of TES-SiO_2 with Ag^+ and Hg^{2+} are:

$$\equiv SiH + Ag^+ + H_2O \rightarrow (\equiv SiOH)Ag^0 + H^+ + \tfrac{1}{2}H_2 \quad (2)$$

$$2(\equiv SiH) + 2Hg^{2+} + 2H_2O \rightarrow 2[(\equiv SiOH)]Hg^+] + 2H^+ + H_2 \quad (3)$$

On the surface of TES-SiO_2 reactions (1), (2) and/or (3) take place in parallel [42]. The observed Hg:H molar ratio is 0.52, which is very close to the average value of 0.49 reported by Katok *et al.*, who worked with amorphous silica and $Hg(NO_3)_2$ solutions [33]. This value is almost half of the theoretical Hg:H molar ratio of 1 dictated by the stoichiometry of the reaction (3). This can be explained by the hydrolysis of hydride according to reaction (1) resulting in less available hydride for reduction.

On the surface of Ag^0@SiO_2 and in the presence of Hg^{2+} amalgamation reactions take place, typically forming schachnerite and moschellandsbergite [34,35,37]:

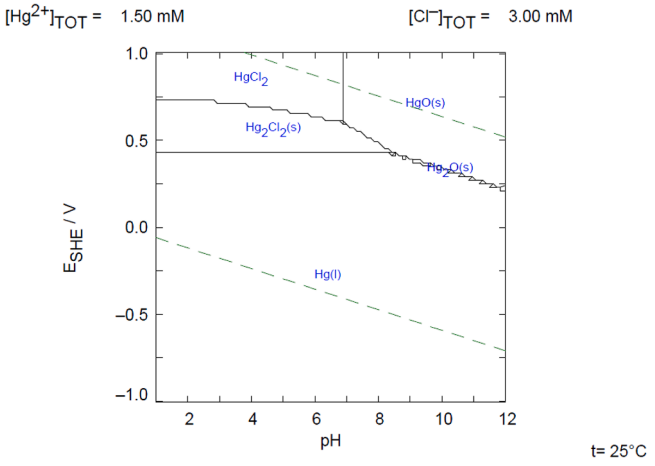

Fig. 13. Pourbaix diagram of mercury in water (Medusa software).

$$Hg^{2+} + 2Ag^0 \rightarrow Hg^0 + 2Ag^+ \quad (4)$$

$$0.9Hg^0 + 1.1Ag^0 \rightarrow Ag_{1.1}Hg_{0.9} \quad (5)$$

$$3Hg^0 + 2Ag^0 \rightarrow Ag_2Hg_3 \quad (6)$$

As mentioned above, the Hg_2^{2+} has been detected on TES-SiO_2 samples in other studies but not on Ag^0@SiO_2, a behavior which has not been explained so far [33,34]. The results show that Hg_2^{2+} is formed on the surface due to reduction of Hg^{2+} followed by the formation of calomel in the presence of Cl^-:

$$2Hg^{2+} + 2Ag^0 \rightarrow Hg_2^{2+} + 2Ag^+ \quad (7)$$

$$Hg_2^{2+} + 2Cl^- \rightarrow Hg_2Cl_2 \quad (8)$$

The higher Hg:Ag molar ratio for the Hg_2^{2+} reduction in comparison to the Hg^0 reduction results in higher removal efficiency. Finally, on the surface of Ag^0@SiO_2, following the oxidation and dissolution of Ag^0, a reaction between Ag^+ and Cl^- takes place [44]:

$$2Ag^0 + ½O_2 \rightarrow Ag_2O \quad (9)$$

$$Ag_2O + 2H^+ \rightarrow 2Ag^+ + H_2O \quad (10)$$

$$Ag^+ + Cl^- \rightarrow AgCl \quad (11)$$

The Ag@SiO_2 samples showed extraordinary efficiency in terms of Hg:Ag molar ratio, which was between 2.28 and 3.02, considerably higher than the stoichiometric ratio of 1 (reaction 7) and the values reported by Katok *et al.*, between 0.29 and 1.70, for a amorphous silica in $Hg(NO_3)_2$ and $Hg(OAc)_2$ solutions [33]. A conservative explanation of this phenomenon is the adsorption of Hg^{2+} on the surface precipitates and possibly the existence of some residual H^- on the surface facilitating the Hg^{2+} removal. A more interesting scenario is the production of excess Hg_2^{2+} beyond the conventional stoichiometry, followed by adsorption on the surface precipitates. Such a hyperstoichiometric effect was observed for fumed silica decorated with Ag^0 NPs with size below 31 nm in $Hg(NO_3)_2$ solutions [34]. This is in good correlation with the average Ag^0 NPs size observed in the current study, between 22 and 25 nm. Clearly, such a hypothesis requires additional experiments and surface characterizations, including XPS. Regardless the exact mechanism, it is clear that the presence of Cl^- is beneficial in terms of Hg^{2+} removal, an important observation when it comes to practical applications.

The solution pH plays an important role in the mercury removal efficiency as it can influence both the aqueous mercury speciation and the stability of the silicon-hydride groups according to reaction (1) [33]. The solutions were slightly acidic in all experiments, with a final pH of 3.4 for TES-SiO_2, 4.5–5.5 for Ag@SiO_2 and 6.8 for SiO_2. The Pourbaix diagram of $HgCl_2$ at 300 ppm is presented in Fig. 13. Based on the redox conditions, unless the solution is basic, the reduction of Hg_2^{2+} to Hg^0 is hindered by the presence of Cl^- and the formation of Hg_2Cl_2. The later cannot be reduced to Hg^0 as its redox potential is lower than that of Ag^+ reduction. The formation of Hg_2Cl_2 in the presence of Cl^- was observed by Pasakarnis *et al.* [43] who studied the reduction of Hg^{2+} on magnetite. The authors argue that slower reduction is observed in the presence of chloride, which suppressed the disproportionation of Hg_2^{2+}, while in the absence of chloride the reduction of Hg^{2+} to Hg^0 proceeds through the disproportionation of Hg_2^{2+}. The predominance of Hg_2^{2+} does not mean absence of Hg^0 otherwise the amalgamation reaction would not happen. Although the ≡Si-H group can reduce Hg_2Cl_2 to Hg^0 the latter was not detected on the surface of the TES-SiO_2 sample. This observation is in agreement with previous studies but there is no obvious explanation. Nevertheless, the speciation of mercury in water in combination with surface redox reactions can provide a plausible explanation of the absence of calomel formation in other studies.

It is important to discuss the stability of the products of the surface reactions in the environment. In general, the solubility of precipitates increases with temperature, however temperature variations in the environment is not expected to have much effect on the solubility of AgCl and Hg_2Cl_2. Also, solubility depends on the nature and concentration of ions in the solution; solubility decreases if common ions present in excess and the effect is the opposite in the case of foreign ions [49]. This might be important in the case for instance of seawater, in which case the solubility of both precipitates decreases. Amalgams are not expected to be affected by conditions typically existing in the environment.

Concerning toxicity, the most toxic forms of mercury are its organic compounds, particularly methylmercury and dimethylmercury. These compounds are produced by the reaction of Hg^{2+} with organic substances in the presence of anaerobic bacteria [50–52]. The Hg^{2+} has been proven to be a predominant toxic agent because of its transformation to organic mercury and one of the methods used to inhibit this process is the reduction to Hg^0 [53]. However, Hg^0 and Hg^{2+} (including its methylated forms) are mobile in the environment and toxic to humans. These forms are predominant in the mercury cycle in the environment [54]. Mercury salts, tend to be insoluble, relatively stable and poorly absorbed [55]. Also, they are relatively harmless to humans because membranes act as barriers to ionic species [50]. Mercurous ion (Hg_2^{2+}) salt in the form of calomel (Hg_2Cl_2) is poorly soluble in water and poorly absorbed by the intestinal, although some portion is oxidized to more mobile forms. On the other hand, mercuric ion (Hg^{2+}) chloride ($HgCl_2$) is very soluble in water and if ingested induces toxicity although only 2% is absorbed initially [55]. Metallic Hg is not absorbed through the gut, so it is not toxic when swallowed. However, metallic mercury has high vapor pressure and upon inhalation it is highly toxic because it passes through the human bodies' membranes [50,55]. On the other hand, the vapor pressure of mercury in amalgams is drastically reduced by more than a million times compared to its metallic form [56]. In overall, it can be stated that from human toxicity point of view metallic mercury and dimethylmercury exhibit high toxicity, mercuric chloride and methylmercury high to moderate and mercurous chloride moderate to low [57]. Taking into account that calomel and amalgams are practically insoluble in water and thus stable in the environment it can be concluded that the immobilization of Hg^{2+} by utilizing reduction and precipitation reactions is an attractive method.

3.3. Thermodynamic calculations

Further insights into the possible reactions and mechanism of processes taking place in the systems studied can be provided by thermodynamic calculations. The thermodynamic data available for organosilanes are sparse mainly due to the experimental difficulties of obtaining them. In the paper of Ho and Melius et al [58] although the

Table 2
Standard Gibbs free energy for the reactions that could take place in the systems studied [59].

#	Reaction	ΔG^0_r kJ·mol^{-1}
12	$HSi(OC_2H_5)_3$ (l) + ½O_2 (g) → $Si(OC_2H_5)_3OH$ (l)*	−337
13	$HSi(OC_2H_5)_3 + H_2O$ (l) → $Si(OC_2H_5)_3OH + H_2$ (g)	−100
14	$HSi(OC_2H_5)_3 + Ag^+$ (aq) + H_2O (l) → $Si(OC_2H_5)_3OH$ + Ag (s) + H^+ (aq) + ½ H_2(g)	−117
15	$HSi(OC_2H_5)_3$ + ½Hg^{2+} (aq) + H_2O (l) → $Si(OC_2H_5)_3OH$ + ½Hg (l) + H^+ (aq) + ½ H_2(g)	−182
16	$HSi(OC_2H_5)_3$ + ½Hg_2^{2+} (aq) + H_2O (l) → $Si(OC_2H_5)_3OH$ + Hg (l) + H^+ (aq) + ½ H_2(g)	−117
17	$HSi(OC_2H_5)_3 + Hg^{2+}$ (aq) + H_2O (l) → $Si(OC_2H_5)_3OH$ + ½Hg_2^{2+} (aq) + H^+ (aq) + ½H_2 (g)	−187
18	$HSi(OC_2H_5)_3 + 2Hg^{2+}$ (aq) + $2Cl^-$ (aq) + H_2O (l) → $Si(OC_2H_5)_3OH + Hg_2Cl_2$ (s) + H^+ (aq) + ½H_2 (g)	−377
19	2Ag (s) + Hg^{2+} (aq) → $2Ag^+$ (aq) + Hg (l)	−10
20	2Ag (s) + $2Hg^{2+}$ (aq) → $2Ag^+$ (aq) + Hg_2^{2+} (aq)	−21
21	2Ag (s) + $2Hg^{2+}$ (aq) + $2Cl^-$ (aq) → $2Ag^+$ (aq) + Hg_2Cl_2 (s)	−123
22	2Ag (s) + $2Hg^{2+}$ (aq) + $4Cl^-$ (aq) → 2AgCl(s) + Hg_2Cl_2 (s)	−234
23	2Ag (s) + Hg_2Cl_2 (s) → 2AgCl(s) + Hg (l)	−8.9

* In the paper of Ho and Melius et al. [58] the authors did not clearly explain the physical state of the two siloxanes, however at 298 K TES is a liquid and although triethoxysilanol is an unstable substance, the presence of the hydroxyl group in its structure suggests that it should also be a liquid at 298 K.

thermodynamic parameters reported were calculated rather than obtained experimentally, they were compared with the experimental data available for some organosilanes and proved to be in a good agreement. In our calculations presented in Table 2 we used the following data from this paper for Gibbs free energy of formation, (ΔG^0_f); ΔG^0_f = -724 kJ·mol^{-1} for TES and ΔG^0_f = -1060 kJ·mol^{-1} for its oxidized derivative, triethoxysilanol $(OC_2H_5)_3$Si-OH. The authors could not compare their calculations of ΔG^0_f with the experimental data due to the absence of the latter, but their calculations of ΔH^0_f for these substances were in a good agreement with the published experimental values. The calculations of standard Gibbs free energy ΔG^0_r for several reactions relevant to the systems studied are summarized in Table 2.

The reactions (12) – (18) adequately describe the surface reactions of the TES-SiO_2 sample. It becomes evident considering, for example, the following set of reactions:

$$3(\equiv\text{Si-OH}) + HSi(OC_2H_5)_3 \rightarrow [3(\equiv\text{Si-O-})]\text{Si-H} + 3C_2H_5OH \quad (24)$$

$$3(\equiv\text{Si-OH}) + HO\text{-}Si(OC_2H_5)_3 \rightarrow [3(\equiv\text{Si-O-})]\text{Si-OH} + 3C_2H_5OH \quad (25)$$

$$[3(\equiv\text{Si-O-})]\text{Si-H} + H_2O \rightarrow [3(\equiv\text{Si-O-})]\text{Si-OH} + H_2 \quad (26)$$

Here ≡Si-OH represents the hydroxylated silica surface and ≡Si-O- represents the silica surface modified with TES or triethoxysilanol. Combining ΔG^0_r for the reactions (24), (25) and (26) as follows:

$$\Delta G^0_r = \Delta G^0_{24} - \Delta G^0_{25} + \Delta G^0_{26} \quad (27)$$

gives ΔG^0_{13} for the reaction (13) in Table 2. Thus, the silica surface reactions for which the thermodynamic parameters are unknown can be substituted by the reactions (12) – (18). Several important observations can be made from the analysis of the data in Table 2. The silicon-hydride group is thermodynamically unstable in the presence of water or oxygen and hydrolyzed or oxidized according to reactions (12) and (18), respectively. Although we have not studied the kinetics of these reactions, from the experimental data these reactions seem sufficiently slow to allow the reduction of silver ions rather than conversion to the silanol groups of freshly prepared TES-SiO_2 sample. The silicon-hydride group is capable of spontaneously reducing Ag^+ and Hg^{2+} and Hg_2^{2+} species to the metallic state and/or lower oxidation state in the case of mercury. The redox reactions (19), (20) and (23) between metallic silver and mercury species have low ΔG^0_r and the direction of the process is significantly influenced by the ratio of their activities according to the equation

$$\Delta G^0_r = \Delta G^0_r + RT\ln Q \quad (28)$$

where ΔG^0_r is the Gibbs free energy of reaction, R is the universal gas constant, T is the absolute temperature, Kelvin and Q is the reaction quotient [59]. Since the activity of metallic silver, metallic mercury and their solid chlorides AgCl and Hg_2Cl_2 is unity, the direction of the process depends on the activities of the dissolved silver and mercury ions, ionic strength and the temperature of the solutions. The ionic strength of the solution is known to affect the adsorption of metal cations by inorganic adsorbents such as oxides. Its effect is complex, and increasing ionic strength may enhance their adsorption by decreasing the zeta-potential at the surface [60] or reduce it due to the competition for the adsorption sites especially if the ion binding occurs via the ion exchange mechanism [61]. In the system described in this paper, the main mechanism of mercury removal is a redox reaction between the immobilised silver nanoparticles and dissolved mercury species followed by calomel formation and mercury-silver amalgamation, on which the effect of other ions usually present in fresh or sea water is minor. The reaction quotient for the reactions (19) and (20) is less than unity because $[Hg^{2+}] > [Ag^+]$ and Q = 1 for the reaction (23) meaning that $\ln Q \leq 0$ for these reactions. Thus, increasing the temperature of the medium will make the mercury reduction according to the equations (19) and (20) more thermodynamically favorable and will have little or no effect on the reaction (23). The positive effect of increasing temperature on Hg^{2+} adsorption by silver/quartz nanocomposites has been reported in the literature [62].

However, the presence of chloride ions has a significant effect on these systems making formation of calomel thermodynamically favourable in reactions (21) and (22). It should be noted that the value of ΔG^0_r as a thermodynamic parameter can only be used to estimate the direction of the reaction rather than its kinetics. The proposed mechanism of Hg-Ag interaction in the systems studied is in agreement with the thermodynamic calculations discussed here.

4. Conclusions

High purity synthetic silica from rice husk was produced and efficiently modified with silicon-hydride functional groups followed by direct reduction of Ag^+ and formation of Ag^0 NPs on the surface of the solid. The silicon-hydride modification was confirmed and quantified by iodometric titration, while the Ag^0 NPs formation on the silica surface was validated using XRD and TEM characterizations. The Ag^0 NPs on the surface of silica were spherical with an average size of 22–25 nm. The adsorption studies revealed that the TES-SiO_2 sample efficiently removes Hg^{2+} by precipitation of calomel on its surface, whereas the efficiency of Ag^0@SiO_2 samples is proportional to the silver content. Calomel forms on the surface of Ag^0@SiO_2 samples along with schachnerite ($Ag_{1.1}Hg_{0.9}$) and probably moschellandsbergite (Ag_2Hg_3). TEM showed the formation of hexagonal nanoparticles of schachnerite supporting the XRD results. SEM/EDX mapping confirmed the co-existence of Ag, Cl and Hg on the surface of the materials. A set of surface reactions were proposed based on the removal experimental data, surface characterizations, literature analysis, aqueous phase speciation studies, redox potentials and thermodynamic analysis. The recycling of a common agricultural waste produced in large amounts around the world and its convertion into high purity amorphous silica and efficient mercury adsorbents, create an added value. The combination of commercial adsorbents such as activated carbon with the high reactivity of TES and/or the exceptional selectivity of Ag^0 NPs towards mercury can lead to the design of highly efficient methods for the treatment of wastewater and the remediation of water bodies.

Declaration of Competing Interest

The authors declare that they have no known competing financial interests or personal relationships that could have appeared to influence the work reported in this paper.

Acknowledgements

This research was funded by the Nazarbayev University project "*Noble metals nanocomposites hyper-activity in heterogeneous non-catalytic and catalytic reactions*", Grant Number 110119FD4536 and partly funded by the Science Committee of the Ministry of Education and Science of the Republic of Kazakhstan (Grant No. AP08857007, 2020-2022).

References

[1] Global Mercury assessment (2019). http://www.unep.org/gc/gc22/Document/UNEP-GC22-INF3.pdf.
[2] M.A. Coulter, Coulter, Minamata convention on mercury, Int. Leg. Mater. 55 (3) (2016) 582–616, https://doi.org/10.5305/intelegamate.55.3.0582.
[3] V.M. Yau, P.G. Green, C.P. Alaimo, C.K. Yoshida, M. Lutsky, G.C. Windham, G. Delorenze, M. Kharrazi, J.K. Grether, L.A. Croen, Prenatal and neonatal peripheral blood mercury levels and autism spectrum disorders, Environ. Res. 133 (2014) 294–303, https://doi.org/10.1016/j.envres.2014.04.034.
[4] L. Deng, X. Ouyang, J. Jin, C. Ma, Y. Jiang, J. Zheng, J. Li, Y. Li, W. Tan, R. Yang, Exploiting the higher specificity of silver amalgamation: Selective detection of mercury(II) by forming Ag/Hg amalgam, Anal. Chem. 85 (2013) 8594–8600, https://doi.org/10.1021/ac401408m.
[5] H.H. Eriksen, F.X. Perrez, The Minamata convention: A comprehensive response to a global problem, Rev. Eur. Comp. Int. Environ. Law. 23 (2) (2014).
[6] H. Qi, W. Xu, J. Wang, L. Tong, T. Zhu, Hg0 removal from flue gas over different zeolites modified by FeCl3, J. Environ. Sci. (China) 28 (2015) 110–117, https://doi.org/10.1016/j.jes.2014.05.050.
[7] S. Sobhanardakani, A. Jafari, R. Zandipak, A. Meidanchi, Removal of heavy metal (Hg(II) and Cr(VI)) ions from aqueous solutions using Fe2O3@SiO2 thin films as a novel adsorbent, Process Saf. Environ. Prot. 120 (2018) 348–357, https://doi.org/10.1016/j.psep.2018.10.002.
[8] J.-G. Yu, B.-Y. Yue, X.-W. Wu, Q.i. Liu, F.-P. Jiao, X.-Y. Jiang, X.-Q. Chen, Removal of mercury by adsorption: a review, Environ. Sci. Pollut. Res. 23 (6) (2016) 5056–5076, https://doi.org/10.1007/s11356-015-5880-x.
[9] A.K. Meena, G.K. Mishra, S. Kumar, C. Rajagopal, P.N. Nagar, Low-cost adsorbents for the removal of mercury (II) from aqueous solution-a comparative study, Def. Sci. J. 54 (2004) 537–548, https://doi.org/10.14429/dsj.54.2067.
[10] J. Kluczka, Reactive polymers in mercury removal from electrolytic brine, Sep. Sci. Technol. 44 (15) (2009) 3698–3716, https://doi.org/10.1080/01496390903182255.
[11] Z. Huang, Z. Wei, X. Xiao, M. Tang, B. Li, X. Zhang, Nitrification/denitrification shaped the mercury-oxidizing microbial community for simultaneous Hg0 and NO removal, Bioresour. Technol. 274 (2019) 18–24, https://doi.org/10.1016/j.biortech.2018.11.069.
[12] N. Panichev, M.M. Kalumba, K.L. Mandiwana, Solid phase extraction of trace amount of mercury from natural waters on silver and gold nanoparticles, Anal. Chim. Acta. 813 (2014) 56–62, https://doi.org/10.1016/j.aca.2014.01.011.
[13] R. Candeago, K. Kim, H. Vapnik, S. Cotty, M. Aubin, S. Berensmeier, A. Kushima, X. Su, Semiconducting Polymer Interfaces for Electrochemically Assisted Mercury Remediation, ACS Appl. Mater. Interfaces. 12 (44) (2020).
[14] Z. Tauanov, P.E. Tsakiridis, D. Shah, V.J. Inglezakis, Synthetic sodalite doped with silver nanoparticles: Characterization and mercury (II) removal from aqueous solutions, J. Environ. Sci. Heal. 54 (2019) 951–959, https://doi.org/10.1080/10934529.2019.1611129.
[15] Z. Tauanov, V.J. Inglezakis, Removal of iodide from water using silver nanoparticles-impregnated synthetic zeolites, Sci. Total Environ. 682 (2019) 259–270, https://doi.org/10.1016/j.scitotenv.2019.05.106.
[16] G. Blanchard, M. Maunaye, G. Martin, Removal of heavy metals from waters by means of natural zeolites, Water Res. 18 (12) (1984) 1501–1507.
[17] F.-S. Zhang, J.O. Nriagu, H. Itoh, Mercury removal from water using activated carbons derived from organic sewage sludge, Water Res. 39 (2-3) (2005) 389–395, https://doi.org/10.1016/j.watres.2004.09.027.
[18] P.L. Yap, S. Kabiri, D.N.H. Tran, D. Losic, Selective and highly efficient adsorption of mercury, ACS Appl. Mater. Interfaces. (2019), https://doi.org/10.1021/acsami.8b17131.
[19] P.A. Kobielska, A.J. Howarth, O.K. Farha, S. Nayak, Metal–organic frameworks for heavy metal removal from water, Coord. Chem. Rev. 358 (2018) 92–107, https://doi.org/10.1016/j.ccr.2017.12.010.
[20] L. Wang, H. Xu, Y. Qiu, X. Liu, W. Huang, N. Yan, Z. Qu, Utilization of Ag nanoparticles anchored in covalent organic frameworks for mercury removal from acidic waste water, J. Hazard. Mater. (2019), 121824, https://doi.org/10.1016/j.jhazmat.2019.121824.
[21] Y.a. Li, C. Wang, S. Ma, H. Zhang, J. Ou, Y. Wei, M. Ye, Fabrication of hydrazone-linked covalent organic frameworks using alkyl amine as building block for high adsorption capacity of metal ions, ACS Appl. Mater. Interfaces. 11 (12) (2019) 11706–11714.
[22] D. Shetty, S. Boutros, A. Eskhan, A.M. De Lena, T. Skorjanc, Z. Asfari, H. Traboulsi, J. Mazher, J. Raya, F. Banat, A. Trabolsi, Thioether-crown-rich calix[4]arene porous polymer for highly efficient removal of mercury from water, ACS Appl. Mater. Interfaces. 11 (13) (2019) 12898–12903.
[23] S. Azat, Z. Sartova, K. Bekseitova, K. Askaruly, Extraction of high-purity silica from rice husk via hydrochloric acid leaching treatment, Turkish J. Chem. 43 (2019) 1258–1269, https://doi.org/10.3906/kim-1903-53.
[24] A. Merkel, A. Satayeva, F. Cannon, C. Howell, S. Meikle, K. László, V. Inglezakis, J. Jandosov, S. Ray, Z. Mansurov, S. Mikhalovsky, Characterisation of activated carbons obtained from rice husk, Eurasian Chem. J. 18 (2016) 299–304. 10.18321/ectj472.
[25] M.C.F. de Cordoba, J. Matos, R. Montaña, P.S. Poon, S. Lanfredi, F.R. Praxedes, J. C. Hernández-Garrido, J.J. Calvino, E. Rodríguez-Aguado, E. Rodríguez-Castellón, C.O. Ania, Sunlight photoactivity of rice husks-derived biogenic silica, Catal. Today. 328 (2019) 125–135, https://doi.org/10.1016/j.cattod.2018.12.008.
[26] R. Hasan, C.C. Chong, S.N. Bukhari, R. Jusoh, H.D. Setiabudi, Effective removal of Pb(II) by low-cost fibrous silica KCC-1 synthesized from silica-rich rice husk ash, J. Ind. Eng. Chem. 75 (2019) 262–270, https://doi.org/10.1016/j.jiec.2019.03.034.
[27] M.Y. Nassar, I.S. Ahmed, M.A. Raya, A facile and tunable approach for synthesis of pure silica nanostructures from rice husk for the removal of ciprofloxacin drug from polluted aqueous solutions, J. Mol. Liq. 282 (2019) 251–263, https://doi.org/10.1016/j.molliq.2019.03.017.
[28] M. Masih, P. Anthony, S.H. Siddiqui, Removal of Cu (II) ion from aqueous solutions by Rice Husk Carbon-Chitosan Composite gel (CCRH) using response surface methodology, Environ. Nanotechnology, Monit. Manag. 10 (2018) 189–198, https://doi.org/10.1016/j.enmm.2018.07.003.
[29] A.R. Satayeva, C.A. Howell, A.V. Korobeinyk, J. Jandosov, V.J. Inglezakis, Z. A. Mansurov, S.V. Mikhalovsky, Investigation of rice husk derived activated carbon for removal of nitrate contamination from water, Sci. Total Environ. 630 (2018) 1237–1245.
[30] Y. Shen, N. Zhang, Facile synthesis of porous carbons from silica-rich rice husk char for volatile organic compounds (VOCs) sorption, Bioresour. Technol. 282 (2019) 294–300, https://doi.org/10.1016/j.biortech.2019.03.025.
[31] L. Huang, Q. Shuai, Facile approach to prepare sulfur-functionalized magnetic amide-linked organic polymers for enhanced Hg(II) removal from water, ACS Sustain. Chem. Eng. 7 (11) (2019) 9957–9965.
[32] M. Zienkiewicz-Strzałka, A. Deryło-Marczewska, R.B. Kozakevych, Silica nanocomposites based on silver nanoparticles-functionalization and pH effect, Appl. Nanosci. 8 (7) (2018) 1649–1668, https://doi.org/10.1007/s13204-018-0837-2.
[33] K.V. Katok, R.L.D. Whitby, F. Fayon, S. Bonnamy, S.V. Mikhalovsky, A.B. Cundy, Synthesis and application of hydride silica composites for rapid and facile removal of aqueous mercury, ChemPhysChem. 14 (18) (2013) 4126–4133.
[34] K.V. Katok, R.L.D. Whitby, T. Fukuda, T. Maekawa, I. Bezverkhyy, S. V. Mikhalovsky, A.B. Cundy, Hyperstoichiometric interaction between silver and mercury at the nanoscale, Angew. Chemie - Int. Ed. 51 (11) (2012) 2632–2635, https://doi.org/10.1002/anie.201106776.
[35] T. Yordanova, P. Vasileva, I. Karadjova, D. Nihtianova, Submicron silica spheres decorated with silver nanoparticles as a new effective sorbent for inorganic mercury in surface waters, Analyst. 139 (2014) 1532–1540, https://doi.org/10.1039/c3an01279d.
[36] M.A.A. Ganzagh, M. Yousefpour, Z. Taherian, The removal of mercury (II) from water by Ag supported on nanomesoporous silica, J. Chem. Biol. 9 (4) (2016) 127–142, https://doi.org/10.1007/s12154-016-0157-5.
[37] S. Azat, E. Arkhangelsky, T. Papathanasiou, A.A. Zorpas, A. Abirov, V.J. Inglezakis, Synthesis of biosourced silica-Ag nanocomposites and amalgamation reaction with mercury in aqueous solutions, Comptes Rendus Chim. 23 (2020) 77–92, https://doi.org/10.5802/crchim.19.
[38] T.R. Bartlett, C. Batchelor-Mcauley, K. Tschulik, K. Jurkschat, R.G. Compton, Metal-halide nanoparticle formation: Electrolytic and chemical synthesis of mercury(I) chloride nanoparticles, ChemElectroChem. 2 (2015) 522–528, https://doi.org/10.1002/celc.201402401.
[39] S. Azat, A.V. Korobeinyk, K. Moustakas, V.J. Inglezakis, Sustainable production of pure silica from rice husk waste in Kazakhstan, J. Clean. Prod. 217 (2019) 352–359, https://doi.org/10.1016/j.jclepro.2019.01.142.
[40] T.R. Crompton, Analysis of organoaluminium and organozinc compounds, Pergamon (1968), https://doi.org/10.1016/c2013-0-02104-4.
[41] L.T. Zhuravlev, The surface chemistry of amorphous silica. Zhuravlev model, Colloids Surfaces A Physicochem. Eng. Asp. 173 (1-3) (2000) 1–38, https://doi.org/10.1016/S0927-7757(00)00556-2.
[42] V.A. Tertykh, N.A. Ivashchenko, V.V. Yanishpolskii, S.A. Khainakov, Platinum nanoparticles on the surface of silica modified with silicon hydride groups, Materwiss. Werksttech. 44 (2-3) (2013) 239–243, https://doi.org/10.1002/mawe.201300115.
[43] T.S. Pasakarnis, M.I. Boyanov, K.M. Kemner, B. Mishra, E.J. O'Loughlin, G. Parkin, M.M. Scherer, Influence of chloride and Fe(II) content on the reduction of Hg(II) by magnetite, Environ. Sci. Technol. 47 (13) (2013) 6987–6994, https://doi.org/10.1021/es304761u.
[44] Z. Tauanov, J. Lee, V.J. Inglezakis, Mercury reduction and chemisorption on the surface of synthetic zeolite silver nanocomposites: Equilibrium studies and mechanisms, J. Mol. Liq. 305 (2020) 112825, https://doi.org/10.1016/j.molliq.2020.112825.

[45] M.R. Baren, The Ag-Hg (Silver-Mercury) system, J. Phase Equilibria. 17 (2) (1996) 122–128, https://doi.org/10.1007/BF02665787.
[46] Y. Liu, C.Z. Huang, Real-time dark-field scattering microscopic monitoring of the in situ growth of single ag@hg nanoalloys, ACS Nano. 7 (12) (2013) 11026–11034, https://doi.org/10.1021/nn404694e.
[47] P. Ravines, L. Li, R. McElroy, An electron microscopy study of the image making process of the daguerreotype, the 19th century's first commercially viable photographic process, J. Imaging Sci. Technol. 60 (3) (2016) 305041–3050410.
[48] S. Ilic, A. Alherz, C.B. Musgrave, K.D. Glusac, Thermodynamic and kinetic hydricities of metal-free hydrides, Chem. Soc. Rev. 47 (8) (2018) 2809–2836, https://doi.org/10.1039/C7CS00171A.
[49] G. Svehla, Vogel's Textbook of Macro and Semimacro Quantitative Inorganic Analysis, 5th ed., Longman, 1979.
[50] P. Atkins, T. Overton, J. Rourke, M. Weller, F. Armstrong, M. Hagerman, Shriver & Atkins' Inorganic Chemistry, 5th ed., Freeman, W. H, 2010.
[51] L. Kozin, S. Hansen, Mercury Handbook, The Royal Society of Chemistry, 2013.
[52] M. Guney, Z. Akimzhanova, A. Kumisbek, K. Beisova, S. Kismelyeva, A. Satayeva, V. Inglezakis, F. Karaca, Mercury (HG) contaminated sites in kazakhstan: Review of current cases and site remediation responses, Int. J. Environ. Res. Public Health. 17 (2020) 1–42, https://doi.org/10.3390/ijerph17238936.
[53] L. Wang, D. Hou, Y. Cao, Y.S. Ok, F.M.G.G. Tack, J. Rinklebe, D. O'Connor, Remediation of mercury contaminated soil, water, and air: A review of emerging materials and innovative technologies, Environ. Int. 134 (2020), 105281, https://doi.org/10.1016/j.envint.2019.105281.
[54] U.S., Environmental Protection Agency (EPA), Fate and transport of mercury in the environment, Mercur. Study Rep. to Congr. III (1997) 1–376. https://www.epa.gov/sites/production/files/2015-09/documents/volume3.pdf.
[55] R.A. Bernhoft, Mercury toxicity and treatment: A review of the literature, J. Environ. Public Health. 2012 (2012), https://doi.org/10.1155/2012/460508.
[56] V.K. Harika, V.B. Kumar, A. Gedanken, One-pot sonochemical synthesis of Hg–Ag alloy microspheres from liquid mercury, Ultrason. Sonochem. 40 (2018) 157–165, https://doi.org/10.1016/j.ultsonch.2017.07.008.
[57] L.A. Broussard, C.A. Hammett-stabler, R.E. Winecker, The Toxicology of Mercury, Lab. Med. 33 (2002).
[58] Pauline Ho, Carl F. Melius, Theoretical study of the thermochemistry of molecules in the Si-O-H-C system, J. Phys. Chem. 99 (7) (1995) 2166–2176, https://doi.org/10.1021/j100007a056.
[59] P. Atkins, J. De Paula, Atkins' Physical Chemistry, 10th ed., Oxford University Press, Oxford, 2010.
[60] Jun Jiang, Ren-kou Xu, Su-zhen Li, Effect of ionic strength and mechanism of Cu(II) adsorption by goethite and γ-Al2O3, J. Chem. Eng. Data. 55 (12) (2010) 5547–5552, https://doi.org/10.1021/je100271u.
[61] G. Petruzzelli, F. Pedron, I. Rosellini, E. Tassi, F. Gorini, B. Pezzarossa, M. Barbafieri, Effect of ionic strength on mercury adsorption on contaminated soil, Int. J. Environ. Ecol. Eng. 7 (2013) 345–348. https://waset.org/publications/1564/effect-of-ionic-strength-on-mercury-adsorption-on-contaminated-soil.
[62] R.S. El-Tawil, S.T. El-Wakeel, A.E. Abdel-Ghany, H.A.M. Abuzeid, K.A. Selim, A. M. Hashem, Silver/quartz nanocomposite as an adsorbent for removal of mercury (II) ions from aqueous solutions, Heliyon. 5 (2019), e02415, https://doi.org/10.1016/j.heliyon.2019.e02415.